Fr : ANALYSE EXPERIMENTALE ET SIMULATION NUMERIQUE CFD EN VUE DE L'ETUDE DU REFROIDISSEMENT DES AUBES ROTOR/STATOR : CAS D'UNE TURBINE A GAZ.

« RESULTATS EXPÉRIMENTAUX PARTIELS»

En: EXPERIMENTAL ANALYSIS AND CFD DIGITAL SIMULATION FOR THE STUDY OF THE COOLING OF THE ROTOR / STATOR BLADES: CASE OF A GAS TURBINE.

" PARTIALS EXPERIMENTAL RESULTS "

Ahmed Beniaiche [*1], Adel Ghenaiet [**], Bruno Facchini [***]

[*]Laboratory of Thermal Power Systems, Ecole Militaire Polytechnique, EMP BP17 Bordj El Bahri, 16046, Algiers, Algeria.

[**] Faculty of Mechanical and Process Engineering University of Sciences and Technology Houari Boumediene, BP 32 Bab-Ezouar 16111 , Algiers, Algeria.

[***] DIEF: Department of Industrial Engineering, University of Florence, Florence, Italy.

[1] Correspondence author: Ahmed BeniaicheFax: +213(0) 21 86 34 56 Email: beniaiche_ahmed25@yahoo.fr

Keywords: Blades cooling system, Internal cooling, Blade trailing edge, Thermo-chromic liquid crystals, Heat transfer coefficient, Nusselt Number, Reynolds number, Rotation number.

ABSTRACT

The aero-thermal behavior of the flow field inside 30:1 scaled model reproducing an innovative smooth trailing edge (TE) of shaped wedge discharge duct with one row of enlarged pedestals have been investigated in order to determine the effect of rotation, inlet velocity and blowing conditions effects, for Re = 20000 and 40000 and Ro = 0 –0.23. Two configurations are presented: with and without open tip configurations. Thermo-chromic Liquid Crystals technique is used to ensure a local measurement of the heat transfer coefficient on the blade suction side under stationary and rotation conditions. Results are reported in terms of detailed 2D HTC maps on the suction side surface as well as the averaged Nusselt number inside the pedestal ducts. Two correlations are proposed, for both closed and open tip configurations, based on the *Re, Pr, Ro* and a new non-dimensional parameter based on the position along the radial distance, to assess a reliable estimation of the averaged Nusselt number at the inter-pedestal region. A good agreement is found between prediction and experimental data with about $\pm 10\ \%\ to\ \pm\ 12\%$ of uncertaincy, for the simple form correlation, and and about $\pm\ 16\%$ using a comple form. The obtained results help to predict the flow field visualization and the evaluation of the aero-thermal performance of the studied blade cooling system during the design step.

Keywords: Blades cooling system, Internal cooling, Blade trailing edge, Thermo-chromic liquid crystals, Heat transfer coefficient, Nusselt Number, Reynolds number, Rotation number, correlations.

NOMENCLATURE

A_h	Inlet section area [mm^2]
D_h	Hydraulic diameter [mm]
D	Distance from pedestal's leading edge to inlet section [mm]
d_p	Pedestal width [mm]
d_t	Pedestal thickness [mm]
d_r	Pedestal's distance in model's radial direction [mm]
h	Heat transfer coefficient [$W\,m^{-2}K^{-1}$]
H_1	Initial duct height [mm]
i	Line of the matrix
I	Turbulence intensity
IP	A given region
j	Column of the matrix
k	Thermal conductivity [$W\,m^{-1}K^{-1}$]
dl	Pedestal length [mm]
U_b	Bulk velocity defined at the inlet section [ms^{-1}]
Nu	Nusselt number [--]
Nu_s	Static Nusselt number [--]
p	Static pressure [Pa]
Pr	Prandtl number [-]
P_x/e	Pitchtorib height ratio[--]
$\dot{q}$	Heat flux density [$W\,m^{-2}$]
Re	Reynolds number [--]
Ro	Local rotation number (Rossby number) [--]
s	Blade thickness [mm] or time scale [$a\ second$].
T	Temperature [$°C\ or°\ K$]
U	Velocity [ms^{-1}]

x	Radial direction[--]
Xr	Dimensionaless distance [--]
x/P_x	Dimensionless position [--]
y^+	Dimensionless wall distance[--]
y	Axial direction[--]
z	Rotation axis direction[--]

Greeks

α	Wedge angle of the inclined wall [*deg*]
μ	viscosity [kg m^{-1} s^{-1}]
ρ	Density of coolant [$kg.m^{-3}$]
Ω	Angular velocity [rad s^{-1}]

Acronyms

2D	Two dimensions
3D	Three dimensions
LE	Leading Edge
*L*0	Inlet duct region
*L*1	Trailing edge region
AR	Aspect Ratio
HTC	Heat transfer coefficient
LCT	Liquid crystal thermography
imax	Line ‘s local matrix size
jmax	Column’s local matrix size
TLC	Thermochromic Liquid Crystal
PMMA	Poly Methyl Methacrylate
PIV	Particles image velocimetry
PS	Pressure side
SS	Suction side

Subscripts

Avg	Average

co	Coolant
f	Film
for	Forced convection
hub	The hub region
in	Inlet
loss	Conduction losses
max	Maximum
nat	Natural
sta	Stationary
tip	The tip region
ro	Referred to ambient conditions
w	Wall

INTRODUCTION

The modern manufacturing technologies allowed having gas turbines more powerful [1] and effective due to the enlarged turbine inlet temperature (TIT) thanks to the advanced air cooling systems that allow blades to operate safely below their material strength limit temperature. The thin trailing edges (TE) are manufactured as a converging ducts in order to decrease mass and assure a better aero-foil and aerodynamic quality. Subsequently, this part of the blade is the most critical. The modern design of thin trailing edges arranges for shapes equipped with pedestals in order to increase the internal heat transfer [2]. Unfortunately, this thin trailing region is subject to great aerodynamic, thermal and structural stresses, and this is why the local information on heat transfer is critical in order to prevent, modify and optimize the coolant and to reduce the internal surfaces, and the use of enlarged pedestals have a lengthened shape of the base section and compared to the circular pin fins, they increase the strength, decrease the pressure losses and increase lowly the heat transfer. Many experimental and numerical studies vis-à-vis the use of pedestals and circular pin fins report the effects of shapes and configurations on the heat transfer. Herein is reported many experimental studies vis-à-vis the use of pedestals, and effects of their configurations on the heat transfer (Fig 1.3). For example, Speziale [3, 4] and Hart [5] gave the main contributions to analyse the fundamental configuration of a radial channel of rectangular cross-section in an orthogonal rotation (i.e., with the rotation axis parallel to the channel height) with an outward flow. However, a key finding of the experimental study by Johnston et al. [6] was that moderate spanwise rotation amplifies and damps turbulent stresses on

the so-called unstable and stable channel side, respectively. The pressure field affects significantly the relative fluid flow and turns out from the effect of the Coriolis forces that act on both the peripheral and radial directions in a plane perpendicular to the rotation axis. A first result, secondary flows appeared (i.e., Coriolis vortices) which mainly act on the channel cross-section moving flow from the channel leading side to the channel trailing side at the channel mid height. On the other hand, the fluid layers close to the upper and lower wall are deflected towards the channel leading side. The distribution of the radial velocity component along the channel height is affected by the pressure field. The velocity profile shape is distorted towards a flattened distribution with the increase of the angular velocity, resulting into a Taylor-Proudman regime at the highest rotation rates that is, with velocity maxima found close to the walls instead of being at the channel mid-height. In this regard, to quantify the rotational effects the rotation number, Ro, is introduced. In the open literature, a significant number of contributions in term of flows in rotating cooling channels can be sited. Conversely, if trailing edge specific applications are considered, only a limited number of experimental or numerical contributions are available, and moreover, the majority of the works concerns ducts for nozzle blades.

The effects of accelerating the flow both on the heat transfer and pressure losses in specific trailing edge geometries using pin fins and enlarged pedestals in a converging duct were experimentally analysed by Metzger and Haley [7], Metzger and al. [8, 9]. An important experimental survey was given by Wang et al. [10, 11], in which they performed detailed heat transfer measurements on the endwall surface of pedestals array with the TLC transient technique. With the same experimental method, Taslim et al. [12, 13] provided two experimental contribution by focussing on the effects of jet impingement in a channel with an axial outflow. In the analysed geometry, cooling air from an adjacent passage was impinged on a rib-roughened surface at the PS or at the SS via a series of race-track shape openings and then discharged at the blade trailing edge. The Liquid Crystal Thermography (LCT) was used to study the effects of jet impingement on a rib-roughened surface. The experiments were performed for Ro = 30000 to 50000. For what concerns the results, firstly, the rib-roughened channel showed a significant global HTC augmentation with respect to the baseline smooth case. Beside analysing the effects of different rib arrangements and height, the race-track shape openings were than tilted such in a way that the ow impinged on the test section wall in the vicinity of the rib root with more scrubbing action against the test section ribbed wall. Furthermore, it was proven that the rib arrangement is crucial to maximise the effects of impingement cooling, which benefits also extend to the opposite internal surface of the duct. More recently this author presented a numerical investigation on a similar geometry concerning the optimum arrangement of crossover jets. Hwang and Liu [14, 15], evaluated the heat transfer and pressure losses in trailing edge cooling geometries typical of real blades: wedge and trapezoidal ducts, pin shape and investigated the lateral flow effects. They concluded that the effects of Coriolis and

centrifugal forces on the fluid flow must be taken into account in rotor blade cooling channels. Recently, Facchini et al. [16] performed an experimental analysis about circular pin fins and enlarged pedestals in a converging duct showing the effects of accelerating flow both on the heat transfer and pressure losses in specific trailing edge cooling geometries. Chang and Liu [17], and Rallabandi et al. [18] accomplished experimental thermal analyses in the case of rotor blades channels, on cooling schemes with an axial outflow. The thermal field investigations were accomplished inside a rotating channel of trapezoidal cross-section with flow ejection at the trailing edge through holes [17] or slots [18]. Researchers produced ready-to-use correlations applicable even in complex geometries under rotation.

About the cooling of pin arrays, few attempts could be found that considered the effect of mixed axial-radial inflow as Kulasekharan and Prasad [19] and by Bianchini et al.[20, 21] for variable cross section ducts. It has been concluded that the mixed orientation (radial – axial) has an effect on the heat transfer. Later, complete experimental and numerical analysis of channel geometry similar to the one in [20] was performed by Armellini et al. [22] and Coletti et al. [23]. In these latter studies, the cooling air from an adjacent passage was impinged on a rib-roughened surface at the pressure side (PS) or at the suction side (SS) wall via a series of race-track shape openings. Through particle image velocimetry (PIV) measurements, these authors obtained a deep insight into the flow, characterized by multiple primary and secondary impingements caused by the mutual arrangement of tilted crossing jets and angled ribs. Liquid crystal thermography (LCT) measurements showed the great impact of this complex flow field on the heat transfer coefficient (HTC) distribution, on both channel sides. Moreover, the detailed experimental and numerical aerothermal analysis pointed out the limits of the numerical solver in predicting the very complex flow field that develops inside the channel and hence the thermal performances. Later, Coletti et al. [24] completed the thermal analysis on this device by means of the conjugate heat transfer measurements. In recent times, The turbulent flows inside a rotating channel provided with transverse ribs along one wall was studied by Coletti et al. [25] by means of 2D time-resolved particle image velocimetry for a Re = 15 000 and a Ro = 0.38. The measurement set-up was mounted on the same rotating disk with the test section. As the ribbed wall is heated, both the Coriolis force and the centrifugal force played a role in the fluid dynamics. The mean velocity fields highlighted the major impact of the rotational buoyancy (Buoyancy number Bo = 0.31) on the flow along the leading side of the duct, and the near-wall layers experience significant centripetal buoyancy. The recirculation area behind the obstacles was enlarged to the point of spanning the whole inter-rib space. Also the turbulent fluctuations were significantly altered, and overall augmented, with respect to the non-buoyant case, resulting in higher turbulence levels far from the rib. On the other hand, the centrifugal force had little or no impact on the flow along the trailing wall. Vortex identification, proper orthogonal decomposition, and two-point correlations were used to highlight rotational effects.

Bonnani et al. [26] performed an experimental survey on 30:1 scaled model the heat transfer of a trailing edge cooling system to study the effects of the rotation *Ro* varied from 0 to 0.3, in internal cooling ducts, for a *Re* of 20000, by testing different configurations: smooth, ribs +60° and ribs -60° *with* closed tip and open tip. For flat or ribbed plates with closed tip and open tip, higher peaks of HTC were shown in the stationary case, located near the pedestal leading edge and along the pedestal surface facing the approaching flow, but were shown to decrease with increasing *Ro* number for all configurations. As expected, the presence of ribs induced a global increase in HTC on the wedge section and tests results show that the ribs +60° of open tip outlet condition reaches the most homogeneous heat transfer distribution all over the ribbed heated surface.

Recently, Beniaiche et al. [27, 28 and 29] studied the same geometry used by [19-26], by means of detailed TLC measurements for a Reynolds number in between 10000 and 40000 and stationary conditions [28] and under rotating conditions [27,29]. They provided two correlations of the averaged Nusselt number estimated at the inter-pedestals regions as an exponent function by means of the flow parameters for three studied geometries: smooth, ribs +60° and ribs -60°, with closed and open tip configurations [28] and under rotating conditions only for the case of the ribs +60° geometry[29]. The variant parameters are *Re, Pr* and a new non-dimensional distance (*Xr*) based on the radial position of pedestals [28]. However they took into account the Ro number effectin correlations of [29].

This literature survey highlights that the most critical region the inter-pedestals region of a turbine blade trailing edge. For this purpose, the present contribution aims to give a better assessment for is. Indeed, our present work is based on the same model and is a continuation of the preceding research carried out by [20-29]. This first part targets studying experimentally, for stationary and under rotating conditions, the heat transfer performance of the smooth case surface of the same innovative scheme geometry studied by authors of [20-27].The rotational number is extended to be 0.23 instead of the stationary case in [28], and the value of 0.15 in [29]. For both two configurations; closed tip and open tip, two forms of correlations (simple form and complex form) are proposed to estimate of the averaged Nusselt number, at the inter-pedestal regions. These correlations are very helpful during the design step.

I. CHANNEL GEOMETRY AND TEST CONDITIONS

The investigated geometry reproduces the internal cooling channel of a highly loaded turbine blade, the same described and analyzed by [20-29]. The experimental procedure conducted by Authors at Department of Industrial Engineering, University of Florence, Florence, used two geometries: smooth geometry, reproducing an internal cooling channel of a highly loaded turbine blade (Figure 1).

The discharge duct at the trailing edge region is wedge shaped and includes a row of seven enlarged pedestals. The cooling air is radialy oriented at the inlet section, then, turned at 90° towards the outlet of the trailing edge. The channel used to guide the flow from the radial inlet to the tangential outlet is split in two parts: the *L*0 region and the *L*1 region (Fig 2). The *L*0 region is composed of a constant height channel and a lateral wall of reduced passage area along the radial direction inclined by 10° to the radialy, used to redirect the flow towards the exit trailing edge. The inlet section, placed at the hub section, is rectangular with a hydraulic diameter *Dh*= 58.18 *mm* and has a high aspect ratio (*AR* = 7.25). The *L*1 (Fig.3) region consists of a converging wedge shaped duct with an angle = 10° and initial height *H*1 = 33 *mm*. The seven (07) pedestals of a length of 84 *mm* and a diameter of 12 *mm* are placed inside *L*1 region and equally spaced with a radial wise distance *Px*= 75 *mm (*Fig.*3 (c)).* Two different kinds of tip were tested: one with a closed section and one with 5 holes discharging the fluid at an ambient pressure (Fig. 4c). [27]

An over view of the experimental set up is given by Figure 2 which details the different components of the used experimental set up.

The measurement of the surface temperatures used a wide band Thermo-chromic Liquid Crystals (30C20W supplied by Hallcrest) steady state technique, active from 30°C to 50°C, calibrated in the same optical condition as a real test. The model was made of transparent medium (PMMA Plexiglas), and to ensure the optical access, the crystals were thinned down with water and sprayed with an airbrush. After preparing the scaled 30:1 model, the TLC is carefully painted on the heated foil. The heating element consists in a 25.4 µm thick Inconel Alloy 600 sheet, applied on the test plate with a double sided tape (Figure 3 (1)). The working conditions are to be fixed by the user (Figure 3 (2)). A digital camera served to record a colour bitmap image (1024x768 pixels) from the TLC painted surface on the PC (IEEE-1394 standard). The illuminating system consists in two studio flashes placed in a steady position at the rig (Figure 3 (3)). In the rotating state, the camera and the flashes are fixed on a stand; hence it was necessary to synchronize the measurement chain as shown by Figure 4. To record an image when the tested geometry crosses the visual field of the camera, a laser transducer triggers (electronic device) drives the camera and the flashes based on a trigger circuit. The input signal coming from the laser transducer is a square wave signal (green line Figure 4) that produces a transition with an adjustable delay (blue line Figure 4), necessary to ensure a correct position of the test section in the visual field of the camera in order to illuminate flashes. A digital camera was used to record the colour bitmap image (1296x964 pixels with a physical pixel size of 0.5 mm x 0.5 mm) from the TLC painted surface on a PC (IEEE-1394 standard) (Figure 3 (4)). Data acquisitions (Figure 3(5)) of each single case are used as the entry conditions during the post processing step. A mask picture (Figure 3(6)) is used during the plotting of the 2D maps of HTC. Without a mask picture, the surfaces down the pedestals are less cooled, and will appear

black surfaces, and taken into account during the post-processing step which might lead to an error. The parameter hue (Figure 3(7)) is used to quantify the colour of the painted surface, and its calibration has been performed by replicating the same optical conditions as in real ones, in order to relate the colour of each pixel location to the local wall temperature Tw. The outputs of the post-processing step are the local temperature distribution over the studied geometry (Figure 3(8)), and by knowing the heat losses, the 2D maps of HTC values are plotted with a possibility to estimate the local Nusselt number and an average Nusselt number (Figure 3(9)). [27]

The uncertainty analyses were performed according to the standard of ANSI/ASME PTC 19.1 [30], based on theKline and Mc. Clintock method [31]. Temperature accuracy is ±0.5 K, differential pressure is ±6.9 Pa, mass flow rate is ±2 - 3%, and heat losses are varied from 4% in the low temperature areas up to 16% in the high temperature relative to the maximum heat imposed, and the wall temperature accuracy (the variation of the temperature for repeated tests) is about ± 10%.

I.1 Data reduction

The blade part subject of this study is a component of the first stage of a gas turbine. This component, which present dimension equal to a few centimeters, is continuously in contact with coolant flows of temperatures from 1200Kup to 1700Kand pressures vary from *15* to *45 bar*[27-29]. Exactly reproducing the effective machine conditions, de facto, is impossible. High pressure, high temperature and small dimensions do not give a scientific unswerving. Therefore, the will to obtain less prohibitive conditions imposes a *scaling* of the problem, using the theory of similitude. Measurements obtained from scaled models can be reported to the real object through some non-dimensional parameters such as the Reynolds number, Mach number, Prandtl number,…etc. Therefore, a scaled model can be bigger than the component that reproduces, allowing detailed measurement. The scale is selected taking into account at the same time the non-dimensional parameter and requirement for structural strength. The Prandtl number depends only on the considered gas (dry air in our experiments) and not on temperature. This way, the studied heat transfer phenomenon is not influenced by the scaling of the real geometry, and results will reproduce those of real gas turbine applications. For which the Reynolds and Nusselt numbers are monitored.[28]

During the heat transfer tests the surface is heated by a constant heat flux and exposed to a cooling air flow and a digital image of the investigated surface is acquired. For the data reduction Reynolds number is estimated at the inlet section of the L0 region similarly to Bianchini et al. [20, 21] and Bonnani et al. [26]:

$$Re = (\dot{m} D_h)/(A_h \mu) \quad (1)$$

Where $\dot{m}$ is the mass flow rate at the inlet section, μ the dynamic viscosity of the air evaluated at the film temperature at the inlet section of the L0 inlet region,D_h the hydraulic diameter and A_h the area of the inlet cross-section.

It has been decided to report the Reynolds number definition to the inlet section area instead of evaluating it at each slot, in order to avoid the use of intrusive instruments which may hide a part of the studied areas and by the way lead to losing local information concerning the HTC distribution.

The Heat transfer coefficient is calculated as:

$$HTC = \frac{\dot{q}}{T_w - T_{co}} \quad (2)$$

Where $\dot{q}$, T_w and T_{co} are the heat generated by the Inconel heating foil, the wall temperature and the coolant temperature at the inlet section, respectively. This HTC definition must be corrected by including the thermal losses due to conduction through the solid body as follows:

$$H = \frac{\dot{q} - \dot{q_{loss}}}{T_w - T_g} \quad (3)$$

By taking into account the thermal losses $\dot{q}$ and the heat generated by the Inconel heating foil, the wall temperature $T_w$and coolant temperature T_c, the local HTC is defined as follows:

$$HTC = \frac{\dot{q} - \dot{q_{loss}}}{T_w - T_{co}} \quad (4)$$

The heat losses $\dot{q}_{loss}$ are 4% in low temperature and 16% in high temperature areas, which are calculated on the heated side by knowing the thermal conductivity and the PMMA plate thickness, according to Bianchini et al. [20, 21] and Bonnani et al. [26]:

$$\dot{q}_{loss} = \frac{k}{s} . \frac{T_w - T_{ro}}{1 + k/(s.h_{conv})} \quad (5)$$

$T_{ro}$is the temperature air before going to the blower.

For the stationary case, the natural convection heat coefficient of the coolanth$_{conv}$is 5-25 W/m^{2}K [65, 66]. However, for rotation cases, h_{conv} is calculated knowing the average Nusselt number between the hub and tip sides, as follows:

$$\overline{Nu} = \frac{\overline{Nu}_{hub} + \overline{Nu}_{tip}}{2} \quad (6)$$

Based on the Reynolds number values, the adequate correlation used to estimate the average Nusselt number at the hub and the tip is given according to [32, 33]:

$$\overline{Nu} = \left(0.037\,\mathrm{Re}^{0.8} - 871\right)\mathrm{Pr}^{1/3}\ \text{, for}\ \left\{\begin{array}{c} 0.6 < Pr < 60 \\ 5.10^5 < Re \leq 10^8 \end{array}\right\}, \quad (7)$$

The Reynolds number is estimated at the hub side and the tip side, respectively, as follows:

$$Re = \frac{\rho_{co}.U.L}{\mu_{co}}, \quad (8)$$

With L is the flat plate length of the flat plate that has a width equal to 0.630 m, and U is the linear velocity [$m.s^{-1}$].

The air density and the dynamic viscosity are estimated at the film temperature T_f(300-317 K).

The calculated Reynolds number values, at the hub and tip positions, are higher than the critical value (5.10^5) to get a turbulent flow.

The forced convection heat coefficient, on the outside geometry, is given by:

$$h_{for} = \frac{Nu.k_a}{L} \quad (9)$$

The dimensionless parameter to take into account in order to reproduce the same rotational condition of real engines is the rotation number, defined as:

$$Ro = \frac{\Omega \cdot D_h}{U_b} \approx \frac{\text{Coriolis Forces}}{\text{Inertial Forces}} \quad (10)$$

Where Ω, D_h and U_b are the rotation speed in rd/s; the hydraulic diameter of the inlet section and the Bulk velocity at the inlet section, respectively.

I.2 Assessment of HTC

A specific Matlab program is used to post-process each 2D HTC map. For a given pixel *(i, j)* location of the (L1+L0) regions, an experimental HTC local value h_{expij} is attributed and the local experimental Nusselt number $Nu_{\exp ij}$ is evaluated as follows: [28]

$$Nu_{\exp ij} = \frac{h_{expij}\, D_h}{k_{co}} \quad (11)$$

To estimate the averaged Nu during the post processing procedure, the equivalent of an *IP* region is a matrix composed of i_{max}lines *by* j_{max}columns, that depends on the region size and the real dimensions of the photographed part of the studied geometry in terms of length and width. The *L0* region was considered as a one single matrix. However, *L1*

region was divided into eight regions which are equal to the number of eight inter-pedestals regions. Each region is represented by an equivalent matrix, and the average Nusselt number of each IP region is the sum of all local Nusselt numbers divided by the number of the locations of the IP region.

The heat transfer coefficient accuracy (the variation for repeated tests) is about ±8% to ±12%, using according to the standard of ANSI/ASME PTC 19.1 [30], based on the Kline and Mc. Clintock method [31].

II. RESULTS AND DISCUSSIONS

The measurements of the heat transfer coefficient correspond to a Reynolds number from 10000 to 40000definedwith respect to the hub inlet section and the Rotation number Ro from 0 to 0.23. Two different configurations were tested corresponding to two surfaces: a flat plate with a closed tip, and an open tip having approximately 12:5% of the inlet flow discharged from the tip. The results are reported in terms of detailed 2D maps of heat transfer coefficient on the suction side spanwise profiles inside the L1 region.

In the 2D HTC maps, the x/P_x is a fraction of the radial distance with the origin located on the mid- span of the L1 region, and y/D is a dimensionless distance with the origin located at the left plan of the inlet section. x, P_x, y and D are respectively, the radial distance, the inter-pedestals distance, the axial distance and the distance from pedestal's leading edge to inlet section (D=32 mm).

In order to facilitate the analysis of different phenomena related to the cooling, all the plots have the same color range and the same scale for HTC.

II.1 Stationary conditions

Figures 5 and 6show the 2D HTC maps for Re = 20000 and 40000, respectively, for closed tip (Figure 5(a) and Figure 6(a)) and open tip (figure5 (b) and figure 6(b), under stationary conditions. Figures 5 and 6 highlights that the values HTC are high at the inlet of the L0 region but tend to decrease from hub to tip. Same figures show that all the cooling configurations have some peculiar features, where two regions of low HTC are noticed. The positions of these low HTC regions are illustrated on Figure 5(a). The first is located in the inter pedestal vane near the hub (region P1) and the second is situated near the tip along the redirecting wall. This last low HTC zone disappears for the open tip configuration.

For each region, the low value of HTC is attributed to the recirculation zones [20, 21,22, 24, 28 and 29].In fact, the flow is fully developed after crossing the inlet section of the L0 region [22, 23, and 24] and due to the fact that the region P1 is directly positioned at a turning angle of 90° of the main flow stream, the average velocity in P1 is low. On the

other hand, the size of the recirculation zone at the P1 region reduces the flow cross section; as a result, the heat transfer coefficient is low [24, 28, 34].

For the closed tip configuration, the PIV data provided by Armellini et al. [22] showed the existence of a recirculation zone at that region, which does not allow the coolant flow reaching that region, and as consequence, the heat transfer exchange is less efficient.

The comparison of Figures 5 and 6 demonstrates that the increase of the Reynolds number induces a reduction of the size of these recirculation zones at P1 and near the tip exit. This is related to the increase of the mass flow rate of the coolant and, consequently, its velocity is increased and improves the efficiency of the heat exchange between the coolant air and the heated wall.

It is easy to see, on Figure 6, that the efficiency of the coolant is decreasing along the x/P_x position, which confirms well the proposed explanations.

In fact, the distribution of HTC is not uniform along the L0 region, as seen on Figures 5 and 6 where the regions near the hub are better cooled than those near the tip. In fact, the flow is fully developed inside the L0 region and, as much as the coolant flows inside this region, it interacts with the heated plate causing a decrease of the temperature gradient (coolant - heated wall) and, subsequently, a reduction of the heat transfer efficiency along the radial direction of L0 region. To highlights this explanation, it is interesting to plot the efficiency of the coolant temperature (equation 12), as defined by Gillespie et al. [36] who and Wu et al. [35] stated, both, that this parameter, describing the efficiency of the heat exchange, decreases along the radial direction of the flow.

$$\frac{(T_b - T_w)}{(T_{co} - T_w)} = \text{The efficiency of the coolent temperature potential} \quad (12)$$

Where Tb the bulk temperature, T_w the wall temperature and T_{co} the temperature of the coolant at the inlet section.

Concerning the L1 region, it is possible to see that the high values of HTC are situated at the leading edge of each pedestal around the stagnation point, especially for the regions from P2 to P7. This is due to turbulence enhancement which started at the L0 region and continues in the L1 region. In fact, the redirecting wall at the L0 region reorients and accelerates the coolant towards the L1 region. At the inlet of the L1 region, the cross section of the flow along the y direction is contracted about 10° (Figure 1(d)) leading to increasing the velocity and the turbulence of the coolant flow. After that, when the flow reaches the leading edge of the pedestal, a horse-shoe vortex is created due to the deviation of the approaching boundary layers over the heated plate and the pedestal surface. The horse-shoe enhances the heat exchanges between the main coolant flow and the heated plate, by encouraging more fresh coolant to reach the heated side of the internal geometry, as reported also by Armellini et al. [22] and Wu et al. [35].

The intensity of the heat exchange decreases along the L1 region going from the region P2 towards P8. In fact, the studied case is a case where the temperature of the heated plane remains higher than the film temperature of the coolant which is the common case of the real blades and, as explained before, the cooling capacity of the coolant is reducing as much as moving towards the tip region along the L0 region, due to the interaction with the heated plate and turbulence disturbances. For that reason, the region P2 is crossed by a flow having a lower film temperature compared to the region P8 where due to the interaction of the recirculation zone at the tip region with the coolant, as redirected towards the region P 8, leads to raising more its film temperature and by the way decreases the heat exchange at this region, as reported on figure 8 illustrating the interaction between the recirculation zone at the tip, for closed tip configuration and the coolant flow exiting from P8. Concerning the open tip configuration, this interaction is canceled due to the non-existence of the recirculation zone at the tip region, however, as seen on figure 7, the efficiency of the coolant temperature is lower at position x/Px =-4, which is the position of the flow before it bifurcates into two flows exiting from the holes of the tip and slot P8, respectively.

II.2 Rotation effects:

In the following, 2D HTC maps of the obtained experimental data for a smooth surface using two configurations: closed and open tip are presented, for Re = 20000 and Ro = 0.23. Those of Re = 40000 and Ro = 0.23, will be given in the next section.

The overall flow behavior under rotation condition compared to stationary cases inside the channel can be commented by referring to the 2D HTC maps reported in figure 9(a,b) and figure 5 (a,b).

At first sight, the HTC values under stationary conditions are increased. Inversely, for Ro = 0.23, the flow is deviated much more in the direction of $y < 0$ of the channel than for stationary conditions. The increase of the effect of the Coriolis forces with the augmentation of the rotation number explains this upper deviation of the flow in the central part of the channel towards the exit slots [22,29,34, and 35], and a decrease of the efficiency of the coolant along the radial direction, as illustrated by figure 9, for Ro = 0.23. Also, it can be seen an extension of the recirculation zone near the redirecting wall towards the tip region. In fact, in the static condition, the core flow has a higher inertia; however, in the boundary layers, the flow is slower. Consistently, the former will tend to keep its radial direction while the boundary layer flow will be easily deviated towards TE [22,29,35] that leads to have a single concavity shape of the vector distributions. On the other hand, the extension of high HTC values in the radial direction of the L0 region, compared to the stationary case, is related to the fact that the Coriolis forces acting on the faster core flow induce the *x* component of the pressure

gradient and, along the radial direction, cause an acceleration of the boundary layer flow. The other explanations regarding the development of the boundary layer inside the L0 region remain valid for the rotation case.

Concerning the L1 region, it is remarkable that the intensity of the HTC values is lower, for Ro = 0.23, than the stationary case, however, the extension of the cooled surface is larger for Ro = 0.23 compared to Ro = 0. References [22,34,29 and 37] stated that, for high rotation numbers, and by moving towards the channel trailing edge, the averaged flow structure is further complicated by the flow acceleration imposed by the narrowing of the channel and the horse-shoe structures appear larger and there is an air replacement between the pressure and the suction sides of the pedestals of the L1 region. As reported in [29], there is a reduction in the separated flow structures downstream of each pedestal when moving towards the blade tip. The outflow, at the inter-pedestal passage trailing edge is almost completely axial close to the blade hub for which a wide recirculation zone affects the discharge flow, and recirculation zones appearing on the suction side of each pedestal decreases the passage area of the flow which accelerates the flow over the pressure side, and results in a better cooling of this side. However, the heat exchange between the flow and the heated plate is lower at the suction side of the pedestal due to the recirculation zone. The intensity of heat exchange is shown to decrease along the L1 region as going from the region P2 toward the region P8. In fact, as explained before, the cooling capacity is decreasing as much as the flow moves toward the tip region along the L0 region, because of the interaction with the heated plate and turbulence disturbances in the L0 region. For that reason, the region P2 is crossed by a flow having a lower temperature than the region P8 where the flow is warmer. The recirculation zone at the tip region interacts with the coolant as redirected towards the region P8 by rising its temperature. As the coolant film temperature is higher, the heat exchange decreases at this region.

Further information in Part II of the present study, based on CFD visualizations, may help to understand the aerodynamic behavior of the flow inside the studied geometry, which may support the given explanation.

III. HTC correlations

In the literature of internal heat transfer calculations [32, 33], the common correlations to estimate the averaged Nusselt number are given in the form of equation 13:

$$Nu = C\, Re^{n}\, Pr^{m} \tag{13}$$

This form has the disadvantage of not giving a correct value along the flow direction. As see on figure 7, the efficiency of the coolant is is decreasing along the radial direction of the flow, which supports well the given statement. For this reason, in the following, two different correlations are developed based on HTC local values for estimating the averaged Nusselt number at L1 regions in terms of *Re*, *Ro*, *Pr* and fraction of radial distance (*Xr*), in order to give a

reliable value of the averaged Nusselt number. A fitting function procedure has been applied to L1 region. For each studied Reynolds number tests were repeated six times, so that each data point is the average of six measurements. Over the range of Reynolds numbers all the data points of the two studied geometries (open tip and closed tip) were fitted into a simple correlation and a complex correlation.

III.1 Simple correlation

First, the average Nusselt number is defined only as a function of the Reynolds number and the rotation number. The Reynolds number is between 10000 -40000 and Rossby number from 0 to 0.23. This first simple form of correlation is proposed for a quick estimation of Nusselt number at each PA inter-pedestals region.

$$Nu = (a + b.Ro^c).Re^d \qquad (13)$$

Where *a, b, c and d* are constants to be determined. In fact, because the stationary states results have been taken into account to correlate the Nusselt number, the term $(a + b.Ro^c)$finds its form in order to reproduce both the stationary and the rotating state. In the stationary conditions *Ro* is equal to zero but the Nusselt number cannot be equal to zero if the term $(a + b.Ro^c)$ has been instead chosen to be $(a\,Ro^c)$. [29]

The obtained values of coefficients *a,b,c*and *d* of HTC correlations are summarized in Table 1and Table 2, for the closed tip and open tip, respectively.

Figure 10 illustrates a comparison of the obtained data of the proposed correlations and those obtained experimentally. A good agreement is found between prediction and experimentation, for a uncertainty of about $\mp$10 % to $\mp$12 %.

This first proposed correlation of Nusselt number is limited even it allows a quick estimation of the average and local Nusselt number. As noticed from these results the Nusselt number is varying along the radial distance from hub to tip region, because of changing in the coolant temperature due to interaction with the heated plate and the turbulence. For this purpose, another correlation that takes into account the effect of Reynolds number, Rossby number, Prandtl number and the radial hub to tip distance in the L1 region is presented.

III.2 Complex correlation

The average Nusselt number is correlated as a function of *Re*, *Ro*, *Pr*in addition to the dimensionless radial distance *Xr* . The same procedure has been followed to estimate the average Nusselt number in the pixel matrix of the *L1* region, as explained previously.

$$Nu=(a + b.Ro^c).Re^d\,.Pr^e.Xr^f \qquad (14)$$

With *a, b, c, d, e* and *f* are the constants to be determined for both closed tip and open tip configurations, considering the ranges of Reynolds number 10000 - 40000, Rossby 0 - 0.23, and Prandtl number of coolant estimated at the film

temperature T_f. In fact, the power coefficient of Prandtl number is constrained to be between 0.3 and 0.4 (as used in the fitting function program), which is according to the value found in the open technical literature for the forced convection. The radial dimensionless distance $\left(Xr = \frac{x}{L1\ lenght}\right)$is obtained by dividing the radial distance, starting from the hub to the tip by the $L1$ region length. It is to say that Xr is different from the x/P_x ratio defined in section 3. After defining the different parameters of the proposed correlation and their constraints, a nonlinear multiple variables procedure was used to fit adequate fitting curves defining the actual correlation. The obtained coefficients are presented in Tab. 3.

Figure 11presents the comparison between the proposed correlations and the experimental data for the closed tip and open tip, respectively. Generally, for each Reynolds number the curves are characterized by a decreasing trend along the L1 region from hub to tip. Indeed, higher values are found close to the hub at the region P2, but there are lower values seen at the region P8. This behavior is still valid for all rotations, where it is noticed that the HTC values increase with Rossby number from 0 to 0.23. All fitted curves of Nusselt number's correlation are within an acceptable accuracy for Reynolds number 10000 - 40000, and Rossby number, between 0 – 0.23.

In overall the percentage error is less than 16%. In fact, this good fitting represents a good agreement between the data and the model and we may conclude that the produced correlations may serve in predicting the average Nusselt number for different flow regimes along the radial distance from hub to tip, for Reynolds number in between 10000 – 40000 and Rossby number up to 0.23.

CONCLUSION

In this paper a non intrusive TLC technique is used to study the heat transfer of a wedge shaped discharge duct of an innovative ribbed (smooth surface) gas turbine blade trailing edge cooling system scheme, for two configurations: a closed tip and an open tip. The working conditions re extended to the range of operating conditions of gas turbine applications with Reynolds number in between 10000 - 40000 and a Rosbey number in between 0 - 0.23. The following conclusions can be made:

1. The proposed geometry allowed comparing two different tip configurations deprived of any prodigious modifications concerning structural changes.
2. The cooling effectiveness is shown to be affected by the tip conditions.
3. From 2D HTC distribution maps, some common features are found: two recirculation zones, for the case of closed tip configuration, a first appears at P1 region near the hub, and another one at the tip region. For the open tip configuration, only the one at P1 exists.

4. The size of the recirculation zonesis inversely proportional to the increase of the Re. However, it is proportional to the rise ofthe Ro due to combined effect of centrifugal and Coriolis forces.
5. Coriolis force induces an axial acceleration to the fluid towards the trailing edge, and when combined to the centrifugal forces induces an extension of the low-HTC region near the redirecting wall and produces a global axialization of the flow.
6. The Reynolds number, Rossbey number, Prandtl number and dimensionless radial distance are considered to be sufficient parameters to quantify the heat transfer coefficient in order to evaluate the cooling effectiveness at the pedestals areas.

Acknowledgements:

Our Acknowledgements go to Dr. C. Carcasci, DrL.Bonnani, Dr. A. Andrei of theDepartment of Industrial Engineering, University of Florence Italy, and Dr. A. Armellini, Dr. A. Pascotto and all the staff of Department of Electrical engineering, Managerial and Mechanical, Universita' of the Studies of Udine, for the help and achievement of the present work.

Funding

This research has been supported by the Italian Ministry of Education University and Research.

Conflit of interest

None declared.

REFERENCES

[1] T. Hawksley, Lecture. Adressed by Captain H. Riall Sankey on Heat Engines to the Institution of Mechanical Engineersin November 1917.

[2] Hunt R. J., The History of the Industrial Gas Turbine - Part 1: The First Fifty Years 1940-1990, idgtE, The Institution of Diesel and Gas Turbine Engineers, Bedford Heights, Manton Lane, Bedford MK41 7PH, publication: 582, 2011.

[3] C. G. Speziale, “Numerical study of viscous flow in rotating rectangular ducts,” Journal of Fluid Mechanics, vol. 122, pp. 251– 271, 1982.

[4] C. G. Speziale and S. Thangam, “Numerical study of secondary flows and roll-cell instabilities in rotating channel flow,” Journal of Fluid Mechanics, vol. 130, pp. 377–395, 1983.

[5] J. E. Hart, “Instability and secondary motion in a rotating channel flow,” Journal of Fluid Mechanics, vol. 45, pp. 341–351, 1970.

[6] Johnston, J.P., Halleen, R.M. and Lezius, D.K. 1972. Effects of spanwise rotation on the structure of two dimensional fully developed turbulent channel flow, J. Fluid Mech., Vol. 56, pp. 533-557.

[7] E. Metzger, S. W. Haley, 1982, Heat transfer experiments and flow visualization for arrays of short pin fins, ASME Paper 82GT138.

[8] E. Metzger, R. A Berry ., and J. P. Bronson., 1982, Developing heat transfer in rectangular ducts with staggered arrays of short pin fins. ASME journal of Heat Transfer, pp 104(1):700706, 1982.

[9] E. Metzger, W. B. Shepard, and S. W. Haley, Row resolved heat transfer variations in pinfin arrays including effects of nonuniform arrays and flow convergence. ASME Paper, 86GT132, 1986.

[10] Z. Wang,. Ireland. P. T, and Jones. T. V, 1993, Detailed heat transfer coefficient measurements and thermal analysis at engine conditions of a pedestal with fillet radii. (GT1993329).ASME Turbo Expo, 1993.

[11] Wang. Z , Jones. T. V, Ireland. P. T, and Kohler. S. T, 1994, Measurements of local heat transfer coefficient over the full surface of a bank of pedestals with fillet radii. GT1994307 .ASME TurboExpo, 1994.

[12] M. E. Taslim and T. Li, “Measurements of heat transfer coef- ficients in rib-roughened trailing-edge cavities with crossover jets,” ASME Paper NO-98GT-435, 1998.

[13] M. E. Taslim and A. Nongsaeng, “Experimental and numerical cross-over jet impingement in an airfoil trailing-edge cooling channel,” Journal of Turbomachinery, vol. 133, no. 4, Article ID 041009, 2011.

[14] Hwang. J. J. and Lui. C. C, 1999, Detailed heat transfer characteristic comparison in straight and 90° turned trapezoidal ducts with pinfin arrays. International Journal of Heat and Mass Transfer, V42 pp: 4005–4016, 1999.

[15] Hwang. J. J, and Lui. C. C, Measurements of endwall heat transfer and pressure drop in a pinfin wedge duct. International Journal of Heat and Mass Transfer, V:45 pp:877–889, 2002.

[16] Facchini. B, Carcasci. C, and Innocenti. L, 2003, Heat transfer and pressure drop evaluation in thin wedge shaped trailing edge. ASME GT200338197.

[17] S. W. Chang, T.-M. Liu, S. F. Chiou, and S. F. Chang, “High rotation number heat transfer of rotating trapezoidal duct with 45° staggered ribs and bleeds from apical side wall,” in Proceedings of the ASME Turbo Expo, pp. 909–921, Montreal, Canada, May 2007.

[18] A. P. Rallabandi, Y.-H.Liu, and J.-C. Han, “Heat transfer in trailing edge wedge-shaped pin-fin channels with slot ejection under high rotation numbers,” in Proceedings of the ASME Turbo Expo, pp. 369–380, Glasgow, UK, June 2010.

[19] N. Kulasekharan and B. Prasad.Effect of coolant entry orientation on flow and heat transfer in the trailing region channels of a gas turbine vane. Proceedings of ASME Turbo Expo 2008: Power for Land, Sea and Air, GT2008-50951, 2008.

[20] C. Bianchini, L. Bonanni, C. Carcasci, B. Facchini, and L. Tarchi.Experimental survey on heat transfer in an internal channel of a trailing edge cooling system.65 AssociazioneTermotecnicaItaliana National Congress, 2010.

[21] C. Bianchini, B. Facchini, F. Simonetti, L. Tarchi, and S. Zecchi.Numerical and experimental investigation of turning flow effects on innovative pin fin arrangements for trailing edge cooling configurations. In Proceedings of ASME Turbo Expo 2010: Power for Land, Sea and Air, GT2010-23536, 2010b.

[22] A. Armellini, F. Coletti, T. Arts, and C. Scholtes, "Aerothermal investigation of a Rib-Roughened trailing edge channel with crossing-Jets—part I: flow field analysis," Journal of Turbomachinery, vol. 132, no. 1, Article ID 011009, 2010.

[23] F. Coletti, A. Armellini, T. Arts, and C. Scholtes, 2010, "Aerothermal investigation of a rib-roughened trailing edge channel with crossing jets—part II: heat transfer analysis," Journal of Turbomachinery, vol. 133, no. 3,Article ID 031024.

[24] F. Coletti, M. Scialanga, and T. Arts, 2011, "Experimental investigation of conjugate heat transfer in a rib-roughened trailing edge channel with crossing jets," Journal of Turbomachinery, vol. 134, no. 4, Article ID 041016, 2011.

[25] F. Coletti,1, D. Lo Jacono, I. Cresci,, and T. Arts, 2014,'Turbulent flow in rib-roughened channel under the effect of Coriolis and rotational buoyancy forces', Journal of PHYSICS OF FLUIDS, vol. 26, 045111.

[26] Bonnani. L, Carcasci. C, Facchini. C, and Tarchi. L, 2012, "Experimental survey on heat transfer in a trailing edge cooling System: effects of rotation in internal cooling ducts". ASME Paper GT2012-69638.

[27] A. Beniaiche, A. Bonanni, and C. Carcasci, TLC Measurements of Heat Transfer Under Rotating Conditions at High Reynolds Number In An Innovative Trailing Edge Cooling System, ASME GTIndia 20129560,2013.

[28] A. Beniaiche, C. Carcasci , M. Pievaroli, A. Ghenaiet, B.Facchini, 2015, Heat transfer investigation in new cooling schemes of a stationary blade trailing edge. Applied Thermal engineering Journal, Vol 87, pp: 816-825.

[29] A. Beniaiche, C. Carcasci , M. Pievaroli, A. Ghenaiet, B.Facchini, 2015, Experimental study of a cooling scheme for a turbine blade trailing edge. Power and Energy Journal Part A, Vol. 229 no 8, pp: 832-848.

[30] ASME, 1985, "Measurement Uncertainty" Instrument and Apparatus, Vol. ANSI/ASME PTC 19.1 of Performance Test Code.

[31] Kline. S. J, and Mc Clintock. F. A, 1953, Describing uncertainties in single sample experiments. *Mechanical Engineering*, Vol. 75, pp: 3–8.

[32] M. J. Moran., H. N. Shapiro., Munson. B. R, and D. P. DeWitt., 2002, Introduction to Thermal Systems Engineering : Thermodynamics, Fluid Mechanics, and Heat Transfer, Wiley, John & Sons, Incorporated, edition 1, September 2002, 0471204900, pp:345.

[33] A. Incropera, B. DeWitt, T. Birgman, A. Lavine, 2007, Fundamentals of Heat and Mass transfer, 6th edition, Wiley, London, UK.

[34] M. Pascotto, A. Armellini, L. Casarsa, C. Mucignat, and P. Giannattasio, 2013, Effects of Rotation at Different Channel Orientations on the Flow Field inside a Trailing Edge Internal Cooling Channel, International Journal of Rotating Machinery Vol 2013, Article ID 765142.

[35]Wu H, Liu Y, Xu G, 2013, "Measurements of heat transfer and pressure in a trailing edge cavity of a turbine blade'. Chinese Journal of Aeronautics", Vol 26(2), pp. 294–308.

[36] D. R. H. Gillespie et al, 2000, Detailed flow and heat transfer coefficient measurements in a model of an internal cooling geometry employing orthogonal interesting channels, ASME TurboExpo, May 8-11 Germany, , Munich, Germany.

[37] A. Andreini, C. Bianchini, A. Armellini, L. Casarsa, 2011, Flow field analysis of a trailing edge internal cooling channel, ASME 2011 Turbo Expo: Turbine Technical Conference and Exposition, pp: 1247-1258.

List of figures:

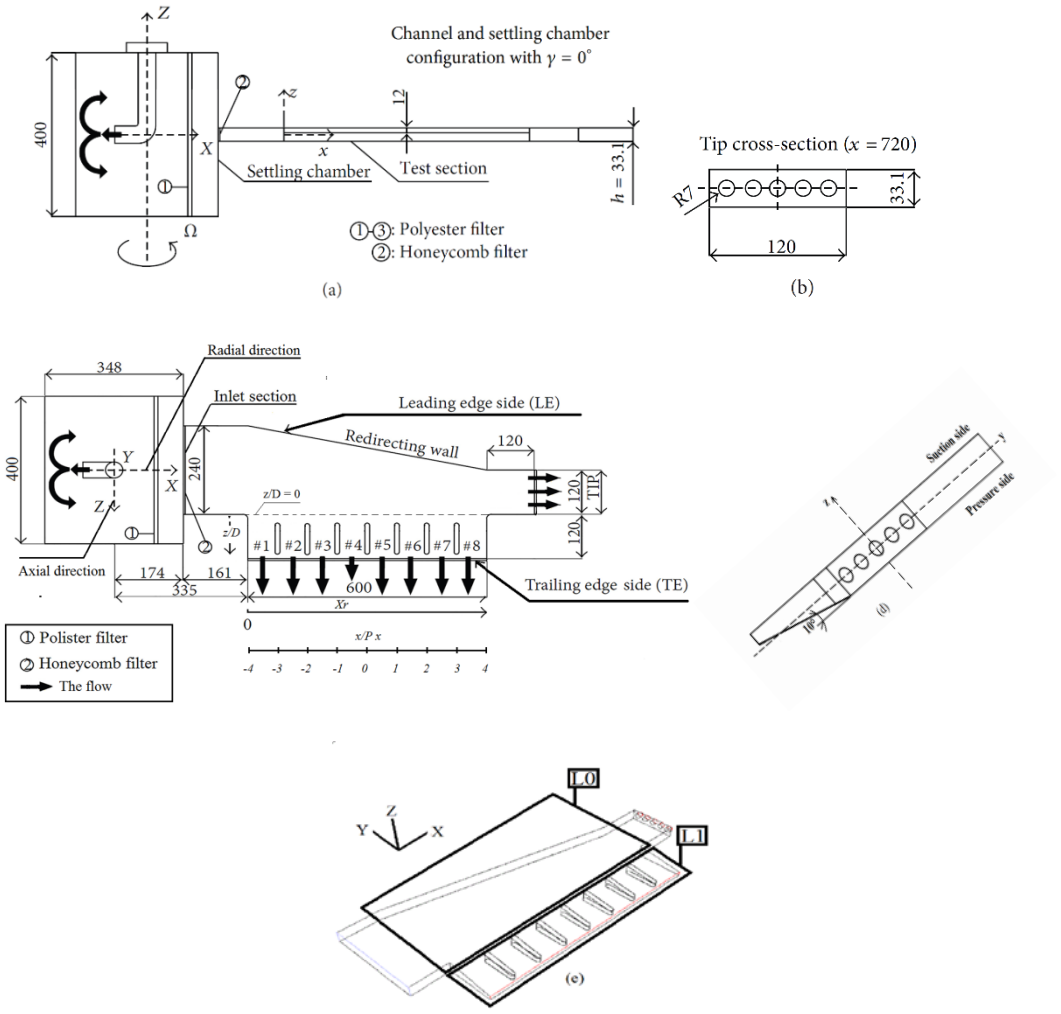

Figure 1 : (a–d) Schematic and (e) 3-D view of the test section investigated in the present study.

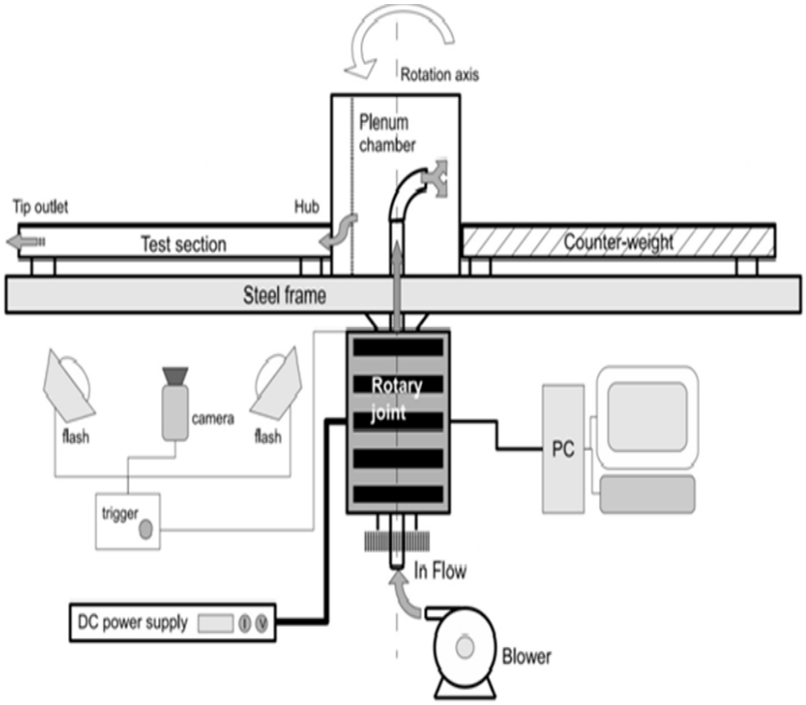

Figure 2 : The test rig.

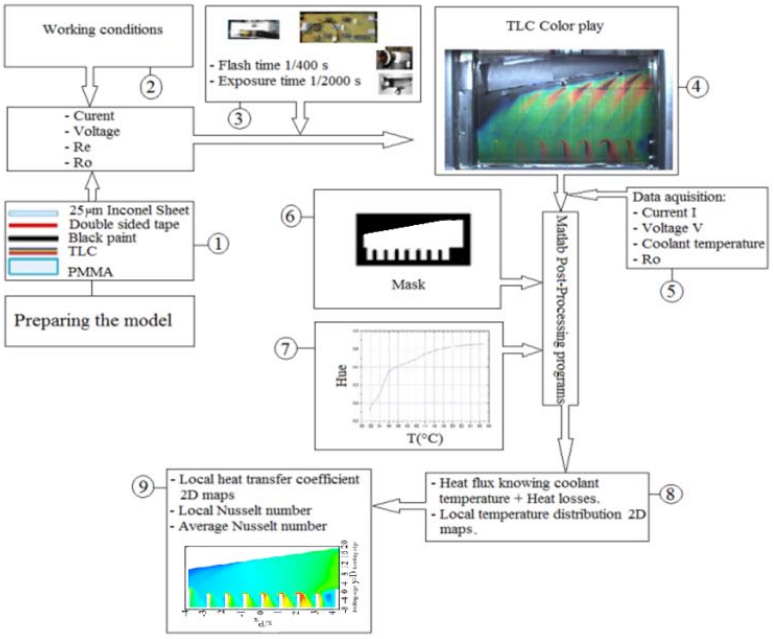

Figure 3: Experimental data acquisition.

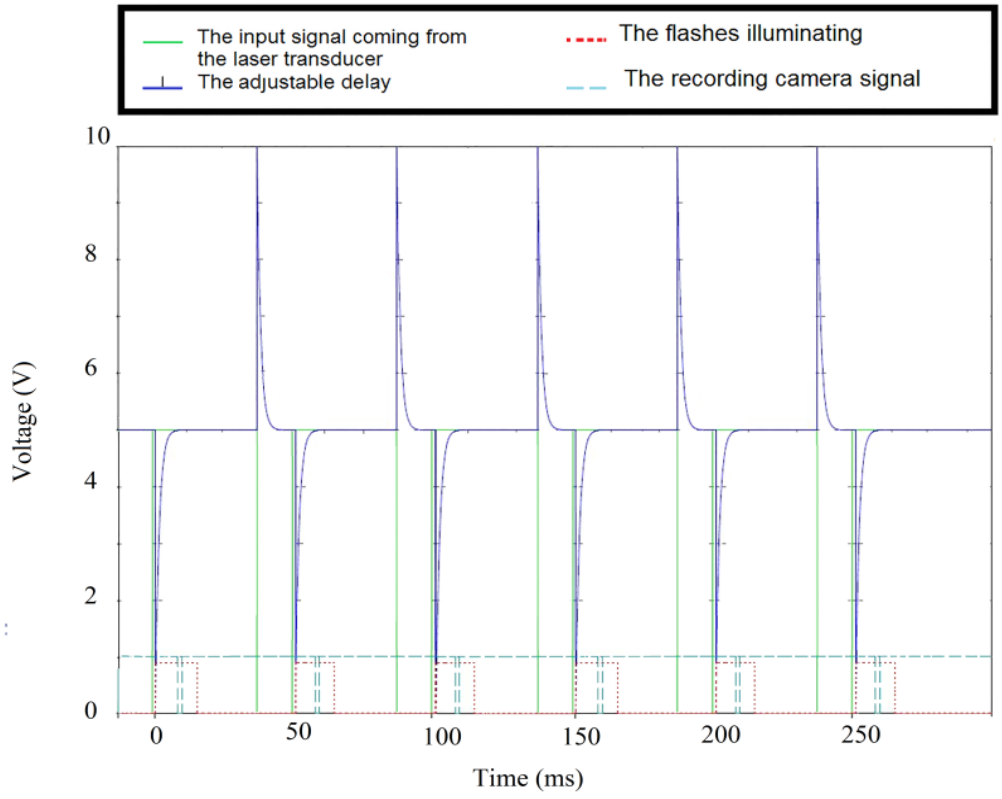

Figure 4: Signal chart.

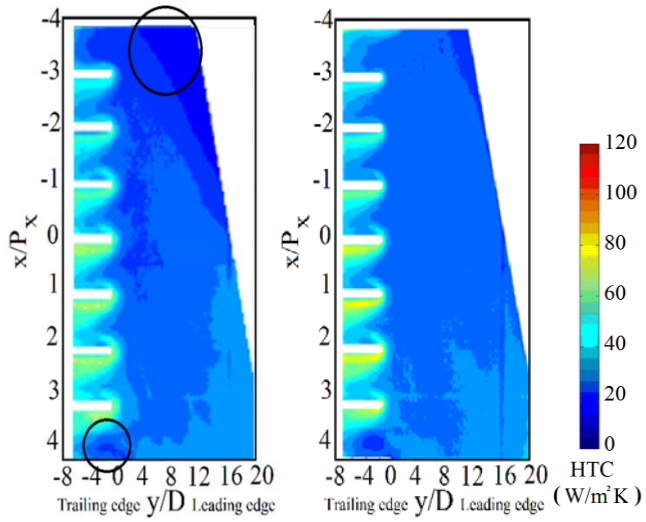

(a) (b)

Figure 5: Comparison of 2D HTC maps (W/m^2K), smooth surface, Re= 20000, Ro = 0,

(a) Closed tip (b) Open tip.

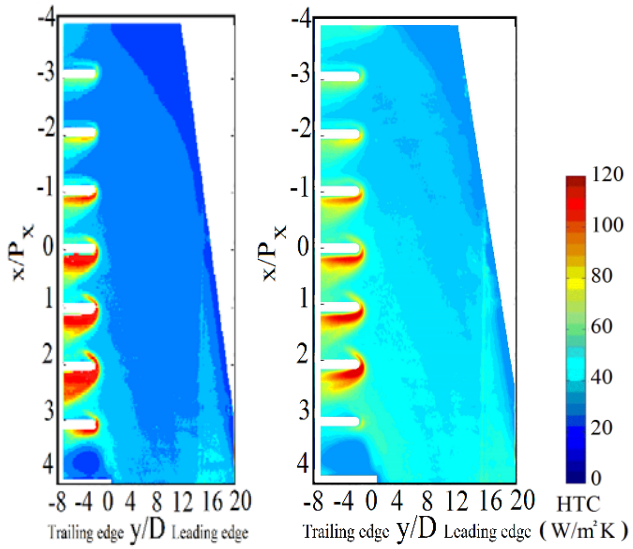

(a) (b)

Figure 6: Comparison of 2D HTC maps (W/m^{2}K), smooth surface, Re= 40000, Ro = 0,

(a) Closed tip (b) Open tip.

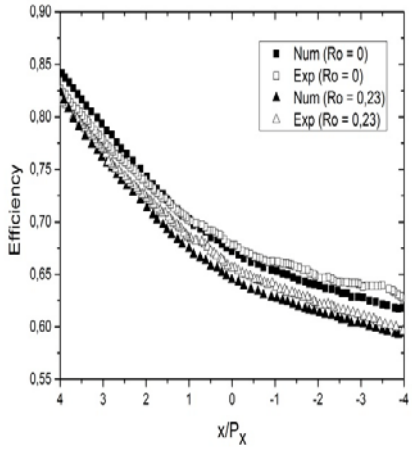

(b)

Figure 7: The coolant temperature potential, Open tip, y/D = - 4, Re= 20000, Ro = 0,

Smooth geometry: Experimental and numerical results.

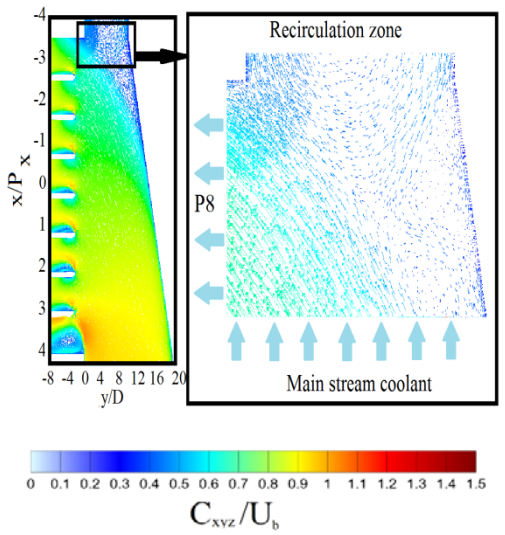

Figure 8 :2D maps of HTC [W/m^2 K]; interaction between the main stream flow and recirculation zone, *xy plane (z=0),* Smooth surface, closed tip, Re=20000, Ro=0.

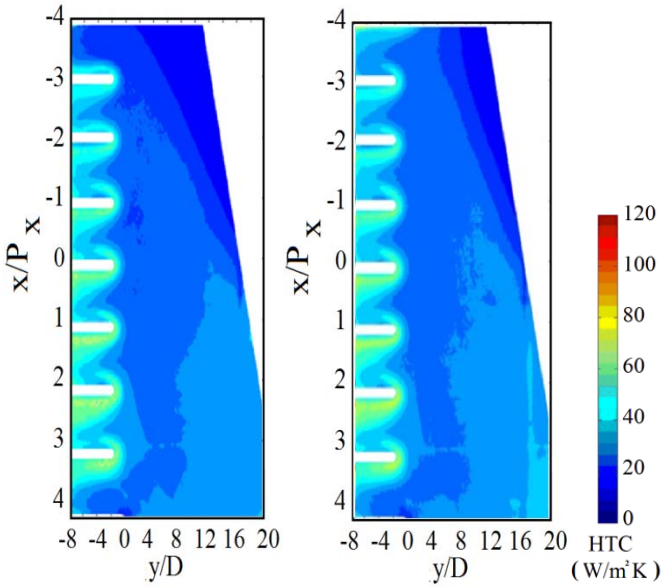

Figure 9: :Comparison of 2D HTC maps (W/m^{2}K), smooth surface, Re= 20000, Ro = 0,23

(a) Closed tip (b) Open tip.

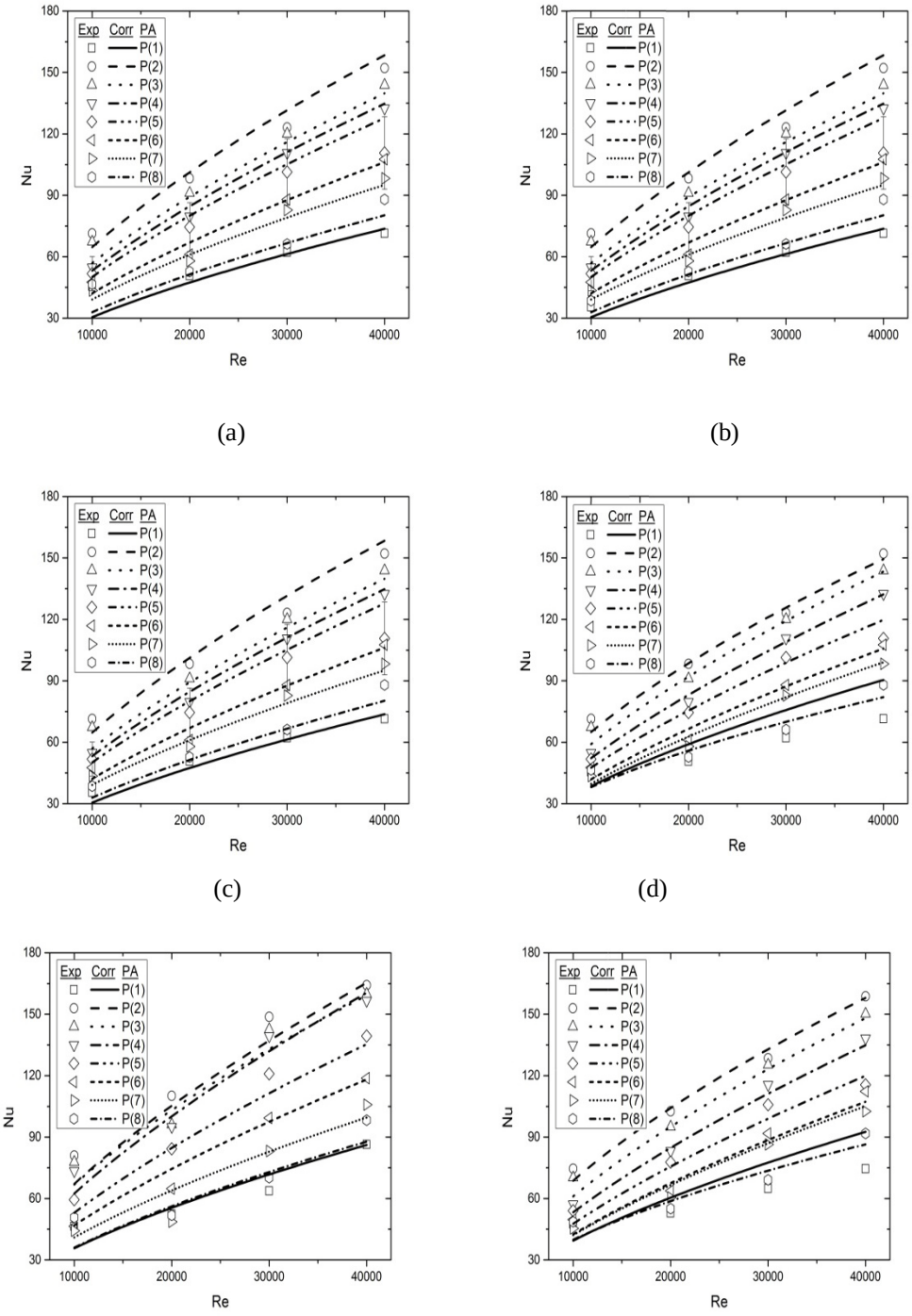

Figure 10 : Comparison of the obtainedsimple correlation data Nu to experimental data for Re=10000-40000:

Closed (a, c,e), Open (b,d,f), Ro =0.00 (a,b), Ro = 0.10 (c,d), Ro = 0.23 (e,f).

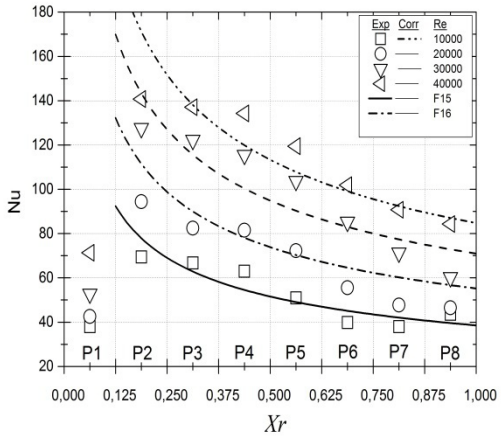

(a)

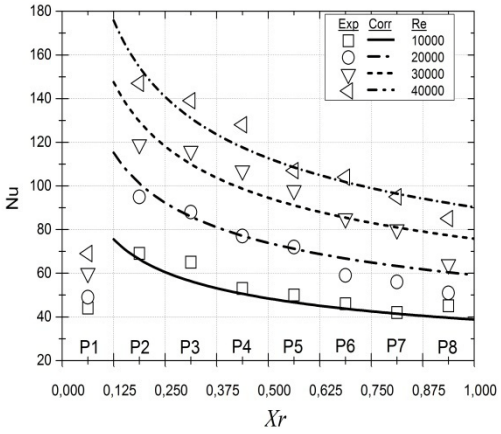

(b)

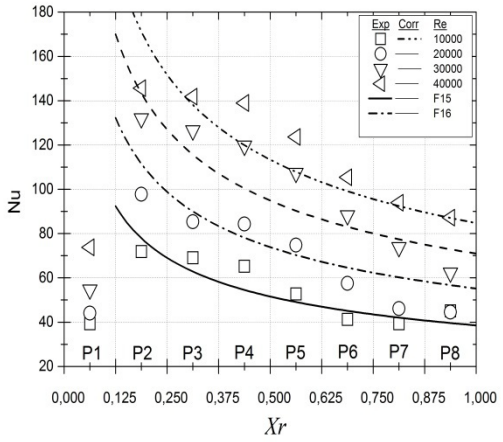

(c)

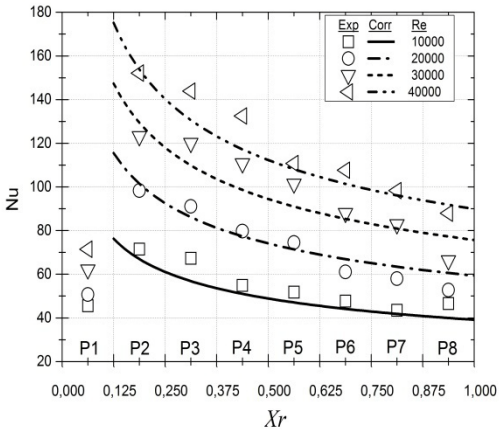

(d)

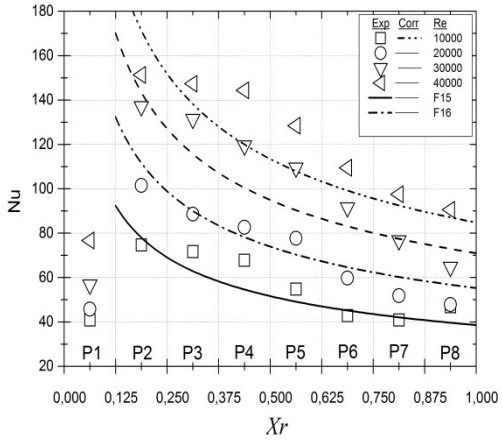

(e)

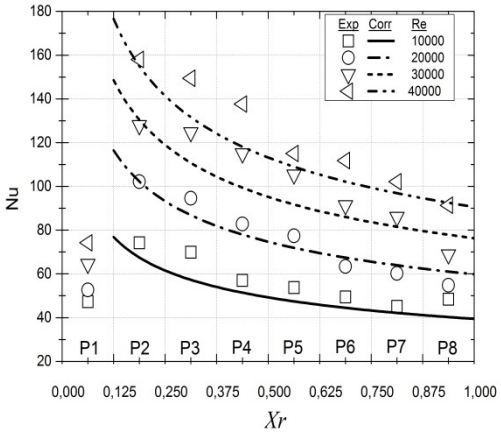

(f)

Figure 11 : Comparison of the obtainedcomplex correlation data Nu to experimental data for Re=10000-40000: Closed (a, c,e), Open (b,d,f), Ro =0.00 (a,b), Ro = 0.10 (c,d), Ro = 0.23 (e,f).

List of tables:

Table 1 : Coefficients for the averaged Nusselt number correlation, closed tip.

Coefficient	Region IP							
	P 1	P 2	P 3	P 4	P 5	P 6	P 7	P 8
a	0.0878	0.1686	0.1456	0.1106	0.1005	0.0911	0.1076	0.0883
b	0.0224	0.0158	0.1052	0.2070	0.0183	0.0861	0.0109	0.0224
c	0.6783	0.3345	0.9981	2.2230	1.0731	1.4473	0.5222	0.6783
d	0.6428	0.6460	0.6481	0.6705	0.6745	0.6663	0.6402	0.6428

Table 2 : Coefficients for the averaged Nusselt number correlation, open tip.

Coefficient	*Region IP*							
	P 1	P 2	P 3	P 4	P 5	P 6	P 7	P 8
a	0.2483	0.1601	0.1601	0.1054	0.1031	0.0871	0.0836	0.2323
b	0.1254	0.5466	0.5466	0.0131	0.0009	0.0082	0.0345	0.0055
c	1.1222	1.2929	1.2929	0.5422	0.8204	0.7323	0.6324	1.9991
d	0.6004	0.6355	0.6399	0.6700	0.6658	0.6686	0.6686	0.5536

Table 3 : Coefficients in Nusselt number correlation

	a	*b*	*c*	*d*	*e*	*f*
Closed tip	0.1390	0.0012	1.6870	0.6182	0.3992	-0.4021
Open tip	0.1630	0.0198	0.1022	0.6002	0.3991	-0.3205